Hormeño, S.; Gregorio-Godoy, P.; Pérez-Juste, J.; Liz-Marzán, L.; Juárez, B.; Arias-Gonzalez, JR. (2014). Laser Heating Tunability by Off-Resonant Irradiation of Gold Nanoparticles. Small. 10(2):376-384. https://doi.org/10.1002/smll.201301912

Laser heating tunability by off-resonant irradiation of gold nanoparticles

Silvia Hormeño,[†,▫] Paula Gregorio-Godoy,[†] Jorge Pérez-Juste,[‡] Luis M. Liz-Marzán,[§,⊥,‡] Beatriz H. Juárez,[†,∥] and J. Ricardo Arias-Gonzalez*,[†,+]*

[†]Instituto Madrileño de Estudios Avanzados en Nanociencia (IMDEA Nanociencia). C/ Faraday 9, Cantoblanco, 28049 Madrid (Spain).

[‡]Department of Physical Chemistry. Universidade de Vigo, 36310 Vigo (Spain).

[§]Bionanoplasmonics Laboratory, CIC biomaGUNE. Paseo de Miramón 182. 20009 Donostia – San Sebastián (Spain).

[⊥]Ikerbasque, Basque Foundation for Science, 48011 Bilbao (Spain).

[∥]Department of Applied Physical Chemistry, Universidad Autónoma de Madrid, Cantoblanco. 28049 Madrid (Spain).

[+]CNB-CSIC-IMDEA Nanociencia Associated Unit "Unidad de Nanobiotecnología".

[▫]Present address: Instituto de Microelectrónica de Madrid, CSIC. C/ Isaac Newton 8, 28760 Tres Cantos, Madrid (Spain).

KEYWORDS. Optical tweezers, thermo-responsive pNIPAM, Au nanoparticles, hydrodynamic size, laser heating

ABSTRACT. Temperature changes in the vicinity of a single absorptive nanostructure caused by local heating have strong implications in technologies such as integrated electronics or biomedicine. We report a detailed study of the temperature changes in the vicinity of a single optically trapped spherical Au nanoparticle encapsulated in a thermo-responsive poly(N-isopropylacrylamide) shell (Au@pNIPAM). Individual beads were trapped in a counter-propagating optical tweezers setup at various laser powers, which allowed us to tune the overall particle size through the phase transition of the thermo-responsive shell. The experimentally obtained sizes measured at different irradiation powers were compared with average size values obtained by dynamic light scattering (DLS) from an ensemble of beads at different temperatures. The size range and the tendency to shrink upon increasing the laser power in the optical trap or by increasing the temperature for DLS agree with reasonable accuracy for both approaches. Discrepancies were evaluated by means of simple models accounting for variations in the thermal conductivity of the polymer, the viscosity of the aqueous solution and the absorption cross section of the coated Au nanoparticle. Our results show that these parameters must be taken into account when considering local laser heating experiments in aqueous solution at the nanoscale. Analysis of the stability of the Au@pNIPAM particles in the trap was also theoretically carried out for different particle sizes.

INTRODUCTION

The study of nanostructures as small sources of heat to locally rise the temperature has acquired great relevance in various fields. For example, in the context of using laser beams for the destruction of tumor tissues through hyperthermia,[1] the development of materials susceptible to release heat upon optical excitation has boosted new therapeutic strategies. To that aim, laser irradiation of metallic nanoparticles (NPs) is a promising concept that requires precise control over parameters that may lead

to deviations in the expected local heating, such as variations in the thermal conductivity or the viscosity of the surrounding medium, at the single particle level.

Metallic NPs absorb electromagnetic radiation and subsequently release energy as heat, thus increasing the temperature of the surrounding medium. The optical properties of the NPs and thus, their ability to generate and confine heat are strongly dependent on their size, shape and surface properties, which has triggered intense synthetic efforts, especially in the case of Au NPs.[2] Heat release is enhanced when a plasmon resonance is excited because electromagnetic energy is strongly absorbed by the metallic NP.[3] However, significant heating (ΔT = 26 ºC at 100 mW) has been determined around Au NPs with 50 nm radius, even if the illumination wavelength lies far away from the plasmon resonance condition.[3b] The heat release from an Au NP under continuous near-IR laser illumination in a thermal bath at room temperature is a non-equilibrium, stationary process that has been previously described.[4] Although the temperature attenuates rapidly down to the ambient level away from the NP, its effect has been measured on lipid bilayers[5] by observing the behavior of fluorescent molecules that have a preference for either fluid or gel phases.

Ultimate applications in therapeutics require not only the knowledge about heat confinement[6] or temperature profile in the vicinity of a single nanostructure, but also studies of the collective behavior of NPs and their biological interaction with tissues, cells or organs.[6-7] However, the characterization of single nanostructures allows us to understand and control processes at the nanoscale such as membrane or DNA melting, drug release or protein denaturation.[5, 8] Hence, the nanoscale thermodynamics of a single Au NP heated by a laser source has gained attention from both experimental and theoretical points of view.[9] Nanoscale thermometry of Au NPs has been addressed by Raman spectroscopy,[10] time-resolved X-ray spectroscopy[11] or by photo-acoustic experiments.[12] Fluorescent molecules,[13] semiconductor NPs[14] and rare-earth compounds[14c] exhibiting temperature-dependent spectra have also been used to estimate the temperature around excited Au NPs.

Thermoresponsive materials, such as poly(N-isopropylacrylamide) (pNIPAM) have also been employed for thermometry. pNIPAM undergoes a phase transition that leads to significant shrinkage of microgel particles upon reaching the lower critical solution temperature (LCST), which can be tuned by several degrees around 32 ºC.[15] For ensembles, the combination of Au NPs with pNIPAM

(Au@pNIPAM) allows not only recording changes in the soft material volume as a consequence of the dissipated heat,[16] but also recording spectroscopic changes in the plasmon resonance of the metallic NPs under optical excitation.[2b, 17]

Single particle experiments provide the means to distinguish individual behavior of molecules, nanoparticles and other nanostructures. In this respect, the use of optical tweezers to trap individual objects[18] is particularly appealing.[19] The first experiments regarding the optical trapping of individual Au NPs were aimed at determining suitable NP sizes and laser wavelengths for a stable trapping.[18a] In previous work, we studied the severe shrinkage of individually trapped pNIPAM beads when they were decorated with 10 nm Au NPs, under 835 nm illumination.[19c] Changes in the plasmon resonance upon laser excitation have also been determined from single particle spectroscopy experiments of individual Au@pNIPAM NPs trapped by single-beam optical tweezers,[2a, 20] and similar experiments were also reported to account for the temperature profile around an individual NP.[5, 7, 21] The aim of this work focuses on an alternative strategy to experimentally and accurately evaluate heating at the nanoscale.

We provide here a detailed analysis of the heat transfer from an individually trapped Au NP encapsulated in a thermo-responsive pNIPAM shell. We use a double counter-propagating optical tweezers set-up, which produces less radiation damage than tweezers formed by a single beam and a more homogeneous spatial intensity profile over the trapped NP. This is particularly convenient for the characterization of soft, active particles.[19c, 22] The mechanical response of the temperature-sensitive material can be used to monitor the radial dependence of the heat transfer outside the NP. In contrast to previous work,[23] in the here reported experiments, no optical plasmon shifts were recorded but rather the thermal fluctuations of individual trapped objects, which yields an indirect measure of their size. Furthermore, we demonstrate that variations in power (ranging from 90 to 120 mW) of the trapping lasers provide control over heating and consequently over the size of the trapped specimen. The size values determined for the trapped objects at different laser powers were compared with those determined by DLS measurements from a colloidal ensemble at different temperatures. This comparison allows us to evaluate the parameters critically influencing the optical trapping measurements, such as water viscosity, thermal conductivity of the shell and absorption efficiency of the embedded Au NPs.

RESULTS AND DISCUSSION

We used a counter-propagating configuration in which two equal beams were brought to the same focus. Figure 1A displays a scheme of the optical trap where the relevant forces are depicted: the scattering and absorption forces push the object in the light propagation direction (F_z), and the gradient force (F_x) drives the object to the highest field intensity region (trap). A weakly focused Gaussian beam with circular polarization, $\mathbf{E}(\mathbf{r})$, and propagating direction $\mathbf{k}$, and its symmetric counter-propagating beam, $\mathbf{E}_c(r)$, with orthogonal circular polarization to prevent interferences, and propagating direction $\mathbf{k}_c = -\mathbf{k}$, meet each other at the common focus. Parameters θ_0, $2z_0$ and $2W_0$ are the beam divergence, the depth of the focus and the diameter of the Gaussian beam, respectively.[24] In our experiments, the wavelength of the beams was λ=835 nm and the numerical aperture of the beams was set to *NA*=0.5, thus giving rise to $2z_0 \approx 3000$, $2W_0 \approx 1000$ nm (see Supporting Information for further details). In this configuration, both absorption and scattering forces in the optical axis cancel out thus affording a 3D trap with weakly focused beams. This configuration increases the amplitude of the position fluctuations in the transversal plane. In contrast, highly-focused laser beams which overfill high numerical aperture (*NA*) objectives provide tight trapping of the NP but reduce the size of the region in which the particle diffuses, thereby reducing the accuracy in the determination of position fluctuations of the particle in the trap.

We selected Au@pNIPAM colloids as a model system because each particle comprises a well-defined metallic NP core homogeneously surrounded by a thermoresponsive polymer shell, so that heat release can be directly monitored through changes in the overall size of the core-shell particle. The Au@pNIPAM colloid was flowed into the optical trapping set-up throughout a fluidic chamber[19c] and individual particles were trapped by the 835 nm lasers. The transmission electron microscopy (TEM) image in Figure 1B clearly shows the contrast between the gold NP cores (dark spots) and the thick, concentric pNIPAM shells (grey annulus). The image shows the high uniformity of the samples, which however contain a few heterogeneities in the form of pNIPAM spheres without Au NP cores or slightly different shaped NPs. The average size of the gold NPs used as cores was determined from statistical analysis of TEM images to be (57 ± 3) nm (see histogram in Figure 1C). Figure 1D shows the

extinction spectra of the sample shown in Figure 1B as an ensemble of particles (not in the trap), at two different temperatures. Heating of pNIPAM leads to a release of water, triggered by a phase transition in the polymer, which changes into a hydrophobic shrunken state upon reaching the LCST. This leads not only to a reduction of the shell volume but also to an increase in its refractive index from n_{pNIPAM} = 1.335 to values that should be near n_{pNIPAM} = 1.410, according to previous literature.[15, 19c, 25] These changes in the optical density of the pNIPAM shell modify in turn the optical response of the Au core, as manifested by a red-shift of the plasmon resonance (black and red lines). In our optical tweezers setup, the wavelength of the lasers (835 nm) is far away from the plasmon resonance and therefore these changes in the extinction spectrum are not significant for the experiments. Figure 1D also shows the calculated extinction efficiency (i.e., the extinction cross section per unit geometrical cross section)[26] for a representative particle (optical constants from ref. 25).[27] This calculation was performed by using the extension of Mie theory to stratified spheres[28] (see Supporting Information). As it can be observed, there is a good agreement between the experimental and the calculated data.

Stability of the particles in the optical trap. The experiment with small composite particles benefits from a symmetric dual-trap optical configuration to provide both a stable trapping (residence time of several seconds) and a significant signal-to-noise ratio for accurate size determination. Since the instant forces in these trapping experiments are near the resolution of the optical tweezers setup (0.1 pN), we performed a theoretical analysis of the optical stability of single particles in the optical trap. This information can be found in the Supporting Information.

The order of magnitude of the theoretical forces in the optical trap is consistent with the experiments in which rapid fluctuating forces below 1 pN could be measured when a particle was in the trap. The ability of the experiments to detect the absorption and scattering effects was ascertained by switching off one of the trapping lasers in the counter-propagating configuration. Under these conditions, the absorption and scattering forces in the axial direction, coming from only one laser, are unbalanced and the particle could not be retained in the optical trap (see Figures S3-S5 for optical stability studies of different Au cores and pNIPAM shell sizes).

Single-particle size measurements.

We inferred the size of individual Au@pNIPAM beads in water from measurements of their drag coefficient by means of the thermal-fluctuation spectral analysis of the force. Briefly, we determined the hydrodynamic size by analyzing the thermal noise of optically-trapped Au@pNIPAM NPs. The equilibrium power spectral density (PSD) of force fluctuations of an overdamped particle in a harmonic potential is given by:[22, 29]

$$\langle \Delta F^2(f) \rangle_{eq} = 2\gamma k_B T f_c^2 / (f^2 + f_c^2)\,, \qquad (1)$$

in units of force squared per frequency, where $\langle \dots \rangle$ represents the ensemble average, $f_c = \kappa/2\pi\gamma$ is the so-called corner frequency, γ is the drag coefficient of the particle, k_B is the Boltzmann constant, T is the temperature, κ is the spring constant of the particle in the optical trap and f is the sampling frequency in units of Hertzs.

The diameter, d, of the Au@pNIPAM microspheres was derived from the drag coefficient ($\gamma = 3\pi d\eta$; where η is the viscosity of the medium). To that end, a voltage signal proportional to the force exerted by the thermal fluctuations of the trapped specimen was recorded and averaged in the frequency domain (see Experimental Section). The resulting data were fitted with the PSD, eq. 1, to obtain the drag coefficient of the Au@pNIPAM microspheres, $\gamma_{Au@pNIPAM}$. The same procedure was used to obtain the drag coefficient of polystyrene microspheres of known diameter, γ_{bead}, which we used for reference experiments. To set d in common units, we calibrated the recorded size of the Au@pNIPAM beads, $d_{Au@pNIPAM}$, relative to that of the reference beads, d_{bead}, from the ratio of the drag coefficients:

$$d_{\mathrm{Au@}pNIPAM} = d_{bead} \times \gamma_{\mathrm{Au@}pNIPAM} / \gamma_{bead}\,. \qquad (2)$$

The weakly focused laser configuration allows measurements at different powers and heating efficiencies. Figure 2 shows the size analysis of Au@pNIPAM beads shown in Figure 1 at three different power values. All the indicated laser powers, both in the experiments and in the simulations, correspond to the total power in the trap, i.e. the sum over the two individual laser powers without

interference term (see Supporting Information). Figure 2A shows the PSD for a single pNIPAM-coated gold NP in the optical trap at (92±1), (113±1) and (120±1) mW. To avoid low- and high-frequency noise, nonlinear regressions were performed for frequencies between ~300 and ~1500 Hz. The information relative to the size of the particles was extracted from the fitting analysis.

The mean values and standard errors for the corner frequency, f_c, friction coefficient, γ, and spring constant, κ, for fitted data like those shown in Figure 2A are shown in Table 1. As expected, the corner frequency increases with the power, which indicates that the optical sensor can follow more rapidly an external stimulus. In the absence of heating, the spring constant should increase with the laser power too, what would indicate that the trap becomes stiffer. However, since the temperature around the particle increases due to the laser heating, the spring constant may decrease with the laser power. Specifically, as the temperature increases, the water viscosity decreases thus making the friction coefficient of the particle, $\gamma = 3\pi d\eta$, decrease; then, as $\kappa=2\pi\gamma f_c$, the balance of the factor γf_c with the laser power determines the behavior of the friction constant. For the gold NP size used in this study, the spring constant of the optical trap slightly increases with power.

In our counter-propagating scheme, the minimum laser power with trapping capacity is 91 mW. The histogram reveals that the mean diameter measured under this power corresponds to (280 ± 103) nm (Figure 2B). Increasing the power to 113 mW yields a mean value of (226 ± 84) nm (Figure 2C). This can be understood as a laser heating effect taking place instantly upon trapping. Further increase in the power (>120 mW) yields histograms with a smaller mean diameter of (184 ± 100) nm and a broader size distribution, most likely due to the higher probability of multiple trapping events (Figure 2D).

The information obtained with the above procedure does not take into account the temperature and viscosity changes in the first water layers around the NPs. In other words, for these experiments we consider the temperature in eq. 1 as the room temperature, which is clearly an oversimplification. For a more accurate explanation of the heating process, we should take into account that upon trapping the temperature around the NP is radially modified with respect to the ambient level, a change that also affects the viscosity of the surrounding medium.

Temperature analysis and laser-induced NP shrinkage. To better illustrate this idea, we show in Figure 3A the temperature increase profile around a 57 nm gold particle illuminated by two counter-propagating 835-nm lasers calculated at three net powers in the optical trap through the following expression:[30]

$$\Delta T(r) = T - T_{\square} = \frac{Q_{abs}}{4\pi r C}\frac{{a_c}^2}{W_0^2}P_{trap}, \quad (3)$$

where r is the distance from the center of the Au NP, T_{∞} is the room temperature, a_c is the radius of the Au core, W_0 is the Gaussian beam width and P_{trap} is the optical power in the focal region, C is the thermal conductivity of the Au NP environment (water for the calculation of Figure 3A) and Q_{abs} is the absorption efficiency of the Au core considering that it is immersed in the pNIPAM/water medium (see Supporting Information for further information). Near the surface of the gold NP, the temperature increment is very high ($\Delta T \approx 46$ ºC at the maximum power used in the optical trap, 126.8 mW) and it decreases rapidly within the pNIPAM shell, thus making the thermal response of the material radially dependent on the distance to the core. It is worth mentioning that such temperature increment on the NP surface is consistent with ΔT values obtained from other measurements made on similar Au NP systems under laser irradiation. In particular, using lipid membranes as temperature sensors, Kyrsting et al. found that the heating at the surface of a 60-nm trapped Au NP is ~523 ºC/W,[21a] which would correspond to $\Delta T \sim$ 66ºC for the highest laser power in our tweezers system. Similarly, the heating associated with the infrared optical trapping of a single 80-nm Au NP embedded in a 2D lipid bilayer is ~385 ºC/W,[5] which leads to $\Delta T \sim$ 49ºC for our laser power. Values within the same range were obtained by Seol et al. who estimated the heating for a 100-nm Au NP to be ~266 ºC/W,[3b] giving rise to an estimate of $\Delta T \sim$ 34ºC at 127 mW.

The pNIPAM shell is heated from the Au core, a process in which the temperature of each concentric layer depends on the radially attenuated heat release from the core. Thus, given that an accurate temperature value for each trapping event cannot be defined, it is more convenient to refer to the laser

power (P_{trap}), rather than to temperature, as the controllable variable in optical tweezers experiments. In the ensemble DLS size determination, in contrast, the phase transition (i.e. collapse) of pNIPAM can be recorded as the temperature is increased. Figure 3B shows the experimental data obtained by DLS from an ensemble of Au@pNIPAM beads. The temperature increase boosts the phase transition and governs the collapse from the swollen state. Mathematically, this behavior can be described by a four-parameter sigmoidal function:

$$D(T) = D_{min} + \frac{D_{max} - D_{min}}{1 + \exp\left(\frac{T - T_{tran}}{\tau}\right)}, \quad (4)$$

where D(T) is the diameter of the composite NP as a function of temperature, D_{min} and D_{max} are the minimum and maximum diameters, respectively, T_{tran} is the midpoint transition temperature (the inflection point of the curve, which can be identified as the LCST), and 2τ is the half-width of the transition. Equation 4 can be used to fit the bulk DLS experimental data in Figure 3B. The quality of the non-linear regression is excellent (see solid curve in Figure 3B, $R^2 = 0.997$) and yields the following values: D_{min} = (233 ± 3) nm, D_{max} = (379 ± 7) nm, T_{tran} = (34.0 ± 0.3) ºC and τ = (2.8 ± 0.3) ºC. The transition width, according to the implicit definition given by eq. 4, is 4τ = 11.2 ºC, the slope being $(D_{max}-D_{min})/4\tau \approx 13$ nm/ºC.

By defining the relative contraction of the pNIPAM material as $\alpha(T) = (D(T)-D_{min})/(D_{max}-D_{min})$, the final size of the Au@pNIPAM NP, D_f, is given by:

$$\frac{1}{2}\left(D_f - D_{min}\right) = \int_{D_{min}/2}^{D_{max}/2} \alpha\left(T(r)\right)\mathrm{d}r = \int_{D_{min}/2}^{D_{max}/2} \frac{\mathrm{d}r}{1 + \exp\left(\frac{T(r) - T_{tran}}{\tau}\right)}. \quad (5)$$

Equation 5 was numerically integrated and the results are plotted in Figure 3C as solid lines.

An analytical expression can be alternatively used within the transition by linearizing eq. 4 for $T \approx T_{tran}$:

$$\alpha^{(l)}(T) \equiv \left.\frac{D(T) - D_{min}}{D_{max} - D_{min}}\right|_{T \approx T_{tran}} = \frac{1}{2}\left(1 + \frac{T_{tran} - T}{2\tau}\right), \quad (6)$$

The result of the linearization is plotted in Figure 3B (black dashed line), showing that it is a good description of the transition. Integration of eq. 6, taking into account the temperature predictions in light trapping experiments for different laser powers (eq. 3), leads to the following expression within the transition:

$$D_f = D_{min} + \frac{1}{2}\left(1 + \frac{T_{tran} - T_\infty}{2\tau}\right)(D_{max} - D_{min}) - \frac{Q_{abs}P_{trap}}{8\pi C\tau}\frac{a_c^2}{W_0^2}\ln\frac{D_{max}}{D_{min}}, \quad (7)$$

Equation 7 predicts the final size of a stratified sphere comprising an Au NP coated by pNIPAM as a function of the optical power in the focus of the laser trap, for a range of laser powers inducing the pNIPAM phase transition. In this way, the combination of bulk DLS measurements with the temperature predictions in light trapping measurements provides a model to account for the single-particle laser-induced NP shrinkage. This analytical expression also shows explicitly the physical parameters that control the shrinkage of the Au@pNIPAM NPs, namely, the Au core radius, a_c, and absorption efficiency, the illumination beam width and wavelength, and the heating transition of pNIPAM.

Note that the absorption efficiency, Q_{abs}, of the Au core and the subsequent pNIPAM shrinkage depend on the refractive index of pNIPAM, n_{pNIPAM}. The black upper lines in Figure 3C account for the final size obtained with $n_{pNIPAM} = 1.38$ and $C = 0.60$ W/m·K (thermal conductivity of water at room temperature) according to eq. 5 (solid line) and its linearization (eq. 7, dashed line).

The dots correspond to the mean sizes measured by single-particle manipulation according to the histograms shown in Figure 2, including viscosity corrections. Temperature variations induced by the Au core influence water viscosity, rendering this correction essential to more accurately estimate the sizes of trapped specimens. As explained in the previous section, the calculated diameter of light trapped specimens is derived from the drag coefficient ($\gamma = 3\pi d\eta$), directly related to the viscosity of the medium η. The influence of η on the final determination of the diameter can be evaluated by using an interpolation formula for viscosity *vs.* temperature,[31] when temperature variations are predicted using expression (3) and diameters from eq. 5. Comparing the size range obtained for single particle

experiments (dots) and the black upper lines obtained from DLS measurements, it is clear that both the range and the tendency to shrink upon increasing the laser power agree with reasonably good accuracy. The surface temperature of an Au NP is a good description of the laser heating effect when the size of the NP is fixed. In our work, the size of the Au@pNIPAM system changes with the laser power and therefore there is not a direct correlation between the laser power and the surface temperature because they are non-linearly dependent. Then, the fact that the mechanical changes experienced by this system are controlled by the laser power is ultimately a consequence of the laser heating effect. Notably, the volume phase transition of the pNIPAM shell was found to be smoother in the laser power coordinate (Figure 3C) than in the temperature coordinate used in the ensemble assays (Figure 3B), which is also a consequence of the radial temperature variation. Specifically, since the temperature decays radially within the pNIPAM shell, adjacent layers of this thermoresponsive material do not contract all at once: the farther the pNIPAM layers from the Au core, the lower the temperature increment and the lower the contraction. The laser power range which tunes the pNIPAM size over its whole contraction range starts with the minimum laser power that triggers the phase transition of the inner layer and ends with the maximum laser power that totally contracts the outer layer. In experiments in which all the pNIPAM layers are in thermal equilibrium (as DLS experiments shown in Figure 3B), all layers contract homogeneously with temperature.

Even if both approaches, namely DLS of an ensemble and individual optical trapping, show a reasonable good agreement, especially at low laser powers, size discrepancies are apparent and larger as the laser power increases. A deep understanding of factors affecting the final heating ability and derived effects in the surrounding medium is mandatory for further applications. Similarly to the previously reported viscosity correction, some other properties from the environment changing upon heating also affect the determination of the final size. In particular, it is possible that the discrepancies are related to the variations in the absorption efficiency of Au@pNIPAM particles and thermal conductivity of the Au NP surrounding medium. To evaluate the influence of these parameters on the size determination, several fittings based on eqs. 5 and 7 have been performed for slightly different values of n_{pNIPAM} and C namely, $n_{pNIPAM} = 1.40$ and $C = 0.55$ W/m·K (middle red lines) and $n_{pNIPAM} = 1.41$ and $C = 0.50$ W/m·K (bottom green lines). The dashed lines in Figure 3C are the linearized curves. These

two cases represent the tendency of the pNIPAM refractive index to increase with temperature[25c, 25d] (as previously mentioned) and that of the thermal conductivity of the Au NP environment to decrease. The latter effect is expected because the thermal conductivity of the polymer is lower than that of water. [32] Since water molecules are released from the polymer network upon heating, the average conductivity of the Au NP environment will be closer to that of the polymer for increasing temperature values. The error bars depicted for the dots correspond to the size range representing a maximum size calculated with (n_{pNIPAM} = 1.38, C = 0.60 W/m·K) and a minimum size calculated with (n_{pNIPAM} = 1.41 and C = 0.50 W/m·K) for each laser power. From the comparison it is clearly observed that better agreement is found from both sets of data when taking into account not only variations in the viscosity but also in the refractive index and conductivity of the surrounding medium. Our results show that by applying a simple analytical expression, the predicted size of trapped specimens can be inferred with reasonably good accuracy.

More accurate predictions could be made taking into account radial variations with temperature for both the thermal conductivity of pNIPAM and its refractive index. This radial dependence, whose rigorous modeling would require a modification of Mie theory for continuous layers, indicates that the inner pNIPAM layers present a higher refractive index since they are heated up to higher temperatures than the outer ones. To this effect, additional experimental evidence should be added, related to the radial dependence of pNIPAM density due to the polymerization process, which increases the difficulty of a more accurate size evaluation.[33] The higher the refractive index of the inner layers, the higher the absorption power of the embedded gold core and the smaller the size of the composite NP (as the most inner layers should transition to the totally shrunken state, see temperature distribution in Figure 3A). All these effects contribute to improve the agreement between the experimental data and the theoretical model in Figure 3C. It is also worth mentioning that single-particle values have been estimated by using a plane wave incidence, whereas the Gaussian is the realistic beam geometry that may contribute to slight differences in the size values. Gaussian beam incidence enhances energy coupling with the NP, thus increasing energy absorption by the metallic NPs (and hence, n_{pNIPAM}) since the beam energy is concentrated in the focal point, where the trapping takes place. All in all, the combination of ensemble

and single particle methods allows characterizing the shrinking behavior of single Au@pNIPAM particles under optical excitation with reasonable accuracy.

CONCLUSIONS

Au@pNIPAM beads with an Au core of *ca.* 60 nm have been characterized by 835-nm optical tweezers. The counter-propagating configuration allows for weak trapping, as well as size determination. Power tuning of the lasers' trap allows for size variation within the size range covering the LCST phase transition. The size values determined by single particle trapping show a reasonably good agreement with those obtained by DLS of an ensemble of particles when taking into account the possible variations produced by changes in the absorption of the Au core, the viscosity of water and the thermal conductivity of the Au surrounding medium.

The Au@pNIPAM particle system shows mechanical changes in response to user-controlled laser power intensities in a wide linear range and at the single particle level. The sharp pNIPAM transitions controlled by temperature are transformed into smoother transitions when they are controlled by laser irradiation since this method does not heat alike all the concentric pNIPAM layers surrounding the Au core.

This knowledge might be useful to optimize the excitation parameters of Au NPs for experiments involving interactions with cell membranes or controlled drug release experiments in biological media. Specifically, our modeling of Au@pNIPAM allows predicting laser-induced mechanical changes within nanometer distances that can be remotely controlled. Moderate heating at the optical trap allows control over the volume phase transition of the beads, which can be very advantageous for applications requiring temperature control at the nanoscale, such us selective heating-induced cell death. ~~Finally,~~ ~~t~~The sensitivity exhibited by the Au@pNIPAM system makes it a good candidate for molecular thermometry, including temperature mapping and control at the nanoscale in studies of fundamental biological processes such as protein folding.[34] Furthermore, detailed understanding of photothermal effects may be relevant to understand elastomeric and glassy liquid crystalline polymer colloids.[35]

EXPERIMENTAL SECTION

Synthesis of pNIPAM-coated Au nanoparticles. The synthesis of Au NPs and further pNIPAM coverage has been performed according to reported methodologies described by Contreras-Cáceres *et al.*[36]

Optical and morphological characterization. UV-vis spectra were recorded using an Agilent 8453 UV-vis spectrophotometer. Dynamic light scattering (DLS) measurements were performed on a Zetasizer Nano S (Malvern Instruments, Malvern UK) with a He–Ne laser operating at 633 nm and a detection angle of 173º (4 mW). The temperature was stabilized for 5 min prior to data acquisition. The intensity averaged particle diameter and the polydispersity index values (an estimate of the distribution width) were calculated from cumulant-type analysis. Transmission electron microscopy was performed by using a JEOL JEM 1010 microscope operating at an acceleration voltage of 100 kV.

Experiments with Optical Tweezers. The optical design includes a dual-counter-propagating-beam (λ = 835 nm) optical trap as published elsewhere.[19c, 37] The two objectives used in this optical tweezers design are Nikon CFI Plan-Apochromat 60X (Nikon Corporation, Tokyo, Japan), water immersion, numerical aperture (*NA*) 1.2. Each objective is used to both focus and collect light for analysis. Laser light exiting the trap is collected and reflected into position-sensitive photodetectors (PD) by using quarter-wave plates and polarizing beam-splitter cubes. Our laser beams were weakly focused (*NA* of the beams, 0.5) to allow significant fluctuations of the trapped particle in the common beam foci. This configuration, in which low-*NA* beams are used inside high-*NA* objectives, allows significant beam deflection while still registering all the scattered light in the PDs, thus increasing the signal-to-noise ratio for the determination of the hydrodynamic size of the particles from the power spectrum analysis. To illuminate the trapped object and follow the experiments by videomicroscopy, we used a blue LED as a light source and Köhler illumination. The image was monitored by a CCD camera (Watec LCL-903K, Edmund Optics). The blue LED has a power of 80 μW measured in front of the lamp and, as it is strongly attenuated, the power at the exit of the first objective in the laser optical path falls to ~300 nW. IR and visible filters are placed in front of the CCD camera to process the images for the different assays.

pNIPAM-coated gold NPs and polystyrene beads used as a control (see main text) were trapped and manipulated with the optical tweezers inside a fluidics chamber. More specifically, they were flowed

into the chamber by an automated fluidics system consisting of glass micro-dispensers and polyethylene tubes connected to the sample reservoirs. As described elsewhere,[19c] a pressure bottle and a glass capillary were used to pump the suspension of particles directly to the main channel of the fluidics chamber. Two other channels were used to flow polystyrene particles of different sizes for control experiments. These channels were connected to the main one by glass capillaries. This design limits the access of different samples to the main channel, where experiments are performed, and allows fast liquid exchanges for experiments under different conditions. It is also very useful to clean channels and remove air bubbles which may cause spurious drift in the force measurements. Channels and pressure bottles were connected through expansion bottles to solenoid valves and pressure sensors whose selection was computer-controlled. To allow switching between opposite flow directions in the channels, one valve was connected to a high pressure source, another to a vacuum source (low pressure) and a third one to atmospheric pressure. Flow rates could be established and stopped with high precision so that sorting and selective trapping of individual specimens were quickly accomplished with high throughput.

Hydrodynamic Size Analysis by Light Trapping. We determined the hydrodynamic size by analyzing the thermal noise of optically-trapped Au@pNIPAM NPs (eq. 1 in the main text). To that end, time-domain voltage signals were recorded in intervals of 5.24 s at 100 kHz. The time interval was then split into 128 parts of 40.96 ms. Next, force fluctuations (in voltage units) in each interval were Fourier transformed in the time domain ($-\infty$, $+\infty$) and averaged over the 128 samples.

Supporting Information Available: Supplementary theory and figures.

Corresponding Authors

* Beatriz H. Juarez: beatriz.hernandez@uam.es

* J. Ricardo Arias-Gonzalez: ricardo.arias@imdea.org

ACKNOWLEDGMENT. This work has been partially supported by Comunidad de Madrid through NANOBIOMAGNET S2009-MAT-1726 and the Spanish Ministry of Science and Innovation through RYC-2007-01709, RYC-2007-01765 and MAT-2009-13488. P. G-G. acknowledges a Research Initiation Grant at IMDEA Nanociencia.

Table 1 Mean values and standard errors for the corner frequency, f_c, friction coefficient, γ, and spring constant, κ, derived from PSD fittings.

Power (mW)	f_c (Hz)	γ (a.u.)[a)]	κ (a.u.)[a)]
120 ± 1	654 ± 20	$(9.52 \pm 0.53)\times10^{-10}$	$(3.91 \pm 0.34)\times10^{-6}$
113 ± 1	600 ± 17	$(1.033 \pm 0.067)\times10^{-9}$	$(3.89 \pm 0.36)\times10^{-6}$
92 ± 1	461 ± 17	$(1.216 \pm 0.096)\times10^{-9}$	$(3.52 \pm 0.41)\times10^{-6}$

[a)] The friction coefficients and spring constants are in arbitrary units because they have been obtained from the PSD, in volts squared per frequency.

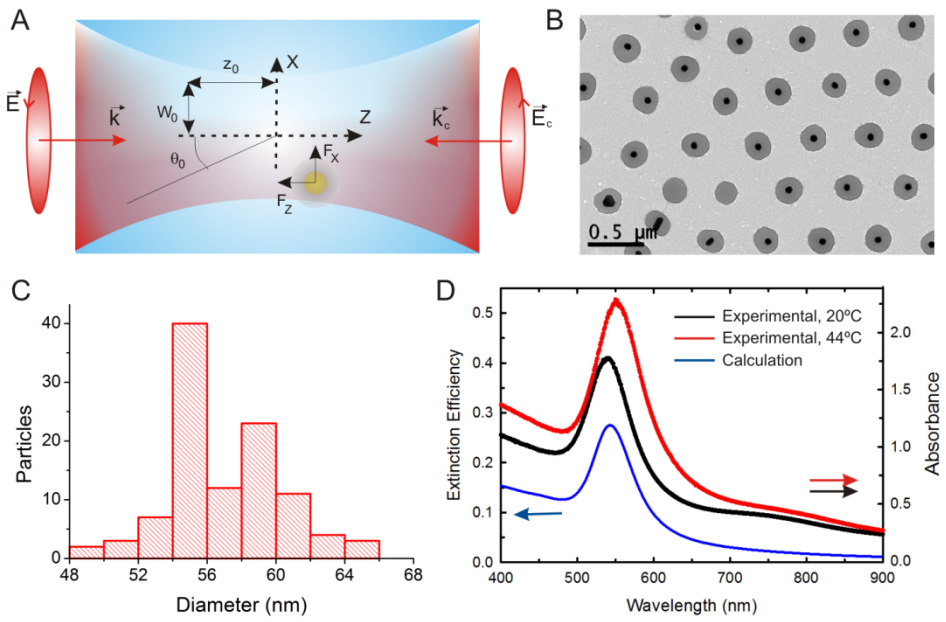

Figure 1 Characterization of the particles in an ensemble. (A) Scheme of the symmetric dual-trap configuration: two Gaussian beams with opposite directions in the optical axis, Z, and opposite circular polarizations in the (X,Y)-plane are weakly focused in the same position. The particle, as illustrated by a yellow-grey concentric circle, experiences a net force towards the center of the trap. Parameters θ_0, z_0 and W_0 characterize the beam profiles (see text for details). (B) Transmission electron microscopy image of Au NPs concentrically covered by pNIPAM. (C) Size distribution of the Au cores of composite particles as derived from TEM images. (D) Absorbance of an ensemble of particles (as those shown in B) in water at two temperatures and calculated extinction efficiency of a 57-nm diameter Au NP coated by a 280-nm diameter pNIPAM spherical shell (refractive index, 1.40) in water.

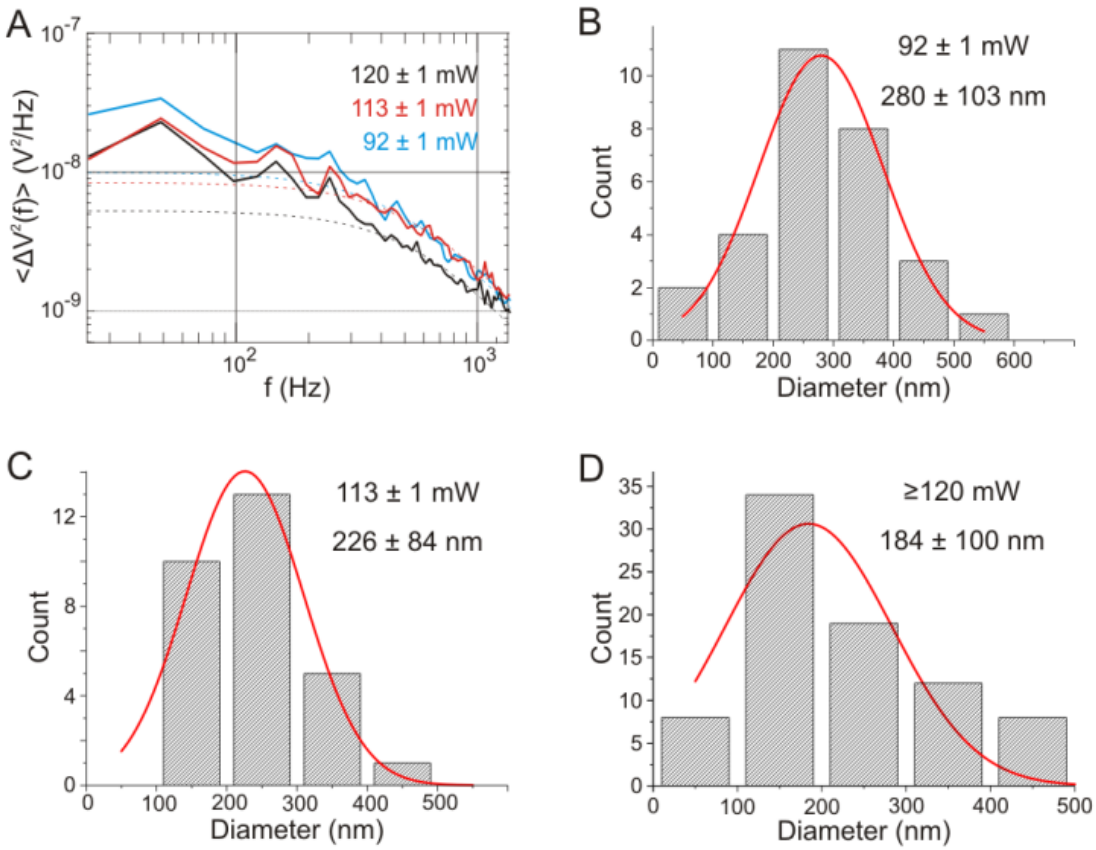

Figure 2 Single-particle characterization. (A) Power spectra for Au@pNIPAM beads (57 nm Au core) trapped at different laser power intensities (the focal region is ~1 μm^2, which yields values in the order of 10^6-10^7 W/cm^2). Dashed curves are fittings to the PSD eq 1. Size distributions in water of the samples measured at 92 mW, 113 mW and 120 mW are shown in (B), (C) and (D) respectively. Red lines in the histograms are Gaussian fits.

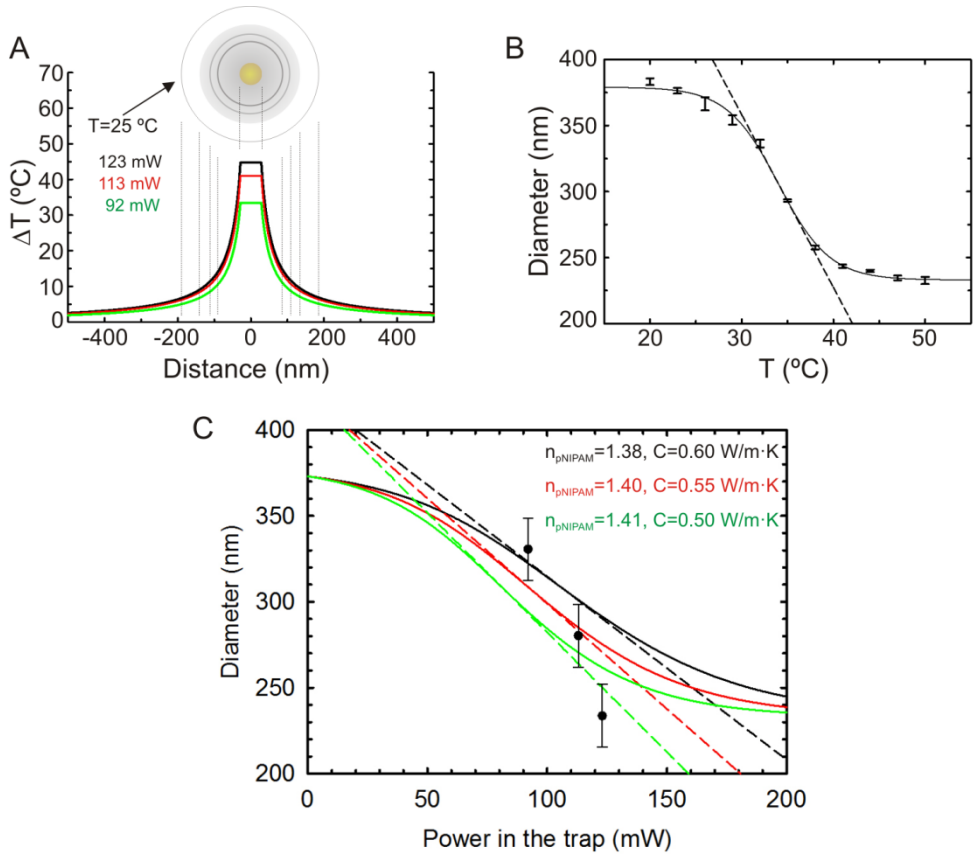

Figure 3 Analysis of the heat-dependent particle size. (A) Temperature increase profile around a 57-nm diameter gold particle illuminated by two counter-propagating 835 nm laser beams, calculated at three net powers in the optical trap. Outer pNIPAM diameters have been extracted from Figure 2. (B) Bulk analysis: a dispersion of particles is heated up and the ensemble-averaged size is plotted as a function of temperature. Black dots, size measurements by DLS; solid line: fit to sigmoidal function, eq. 4; dashed line, linearization in the vicinity of the pNIPAM phase transition (T ≈ Ttran). (C) Single-particle analysis: individual particles are optically trapped and the pNIPAM annulus is heated up radially from the Au core. The black dots are particle size measurements as a function of temperature, corrected from temperature and subsequent viscosity changes on the outer pNIPAM surface (see text for details). Solid line, integrated sigmoidal function, eq. 5; dashed line, integrated linear behavior, eq. 7, in the vicinity of the pNIPAM temperature-induced phase transition (T ≈ Ttran). Three sets of parameters are represented (colors) to account for the influence of C and n_{pNIPAM} variations during the laser heating.

Table of Contents

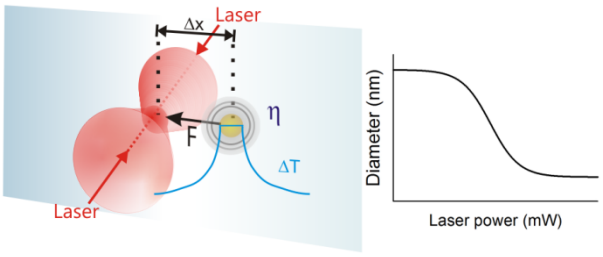

Temperature changes in the vicinity of a single absorptive nanostructure caused by local heating have strong implications in technologies such as integrated electronics or biomedicine. Laser irradiation of Au nanoparticles requires precise control over parameters that may lead to deviations in the expected local heating, such as variations in the thermal conductivity or the viscosity of the surrounding medium. To accurately address the temperature changes in the vicinity of a single nanostructure, Au NPs encapsulated in thermo-responsive shells were individually optically trapped.

REFERENCES

[1] X. Huang, P. K. Jain, I. H. El-Sayed, M. A. El-Sayed, *Nanomedicine* **2007,** *2*, 681.

[2] a) C. M. Pitsillides, E. K. Joe, X. Wei, R. R. Anderson, C. P. Lin, *Biophys J* **2003,** *84*, 4023; b) J. Pérez-Juste, I. Pastoriza-Santos, L. M. Liz-Marzán, P. Mulvaney, *Coordination Chemistry Reviews* **2005,** *249*, 1870; c) R. D. Averitt, D. Sarkar, N. J. Halas, *Physical Review Letters* **1997,** *78*, 4217.

[3] a) J. R. Arias-González, M. Nieto-Vesperinas, *J. Opt. Soc. Am. A* **2001,** *18*, 657; b) Y. Seol, A. E. Carpenter, T. T. Perkins, *Opt Lett* **2006,** *31*, 2429.

[4] A. O. Govorov, H. H. Richardson, *Nano Today* **2007,** *2*, 30.

[5] P. M. Bendix, S. N. S. Reihani, L. B. Oddershede, *ACS Nano* **2010,** *4*, 2256.
[6] Z. Qin, J. C. Bischof, *Chemical Society Reviews* **2012,** *41*, 1191.
[7] P. Haro-Gonzalez, W. T. Ramsay, L. M. Maestro, B. del Rosal, K. Santacruz-Gomez, M. C. Iglesias-de la Cruz, F. Sanz-Rodriguez, J. Y. Chooi, P. R. Sevilla, M. Bettinelli, D. Choudhury, A. K. Kar, J. García Solé, D. Jaque, L. Paterson, *Small* **2013,** *9*, 2162.
[8] J. Do, R. Schreiber, A. A. Lutich, T. Liedl, J. Rodriguez-Fernandez, J. Feldman, *Nano Lett* **2012,** *12*, 5008.
[9] a) H. Goldenberg, C. J. Tranter, *British Journal of Applied Physics* **1952,** *3*, 296; b) V. K. Pustovalov, *Chemical Physics* **2005,** *308*, 103; c) V. K. Pustovalov, V. A. Babenko, *Laser Physics Letters* **2004,** *1*, 516.
[10] H. H. Richardson, Z. N. Hickman, A. O. Govorov, A. C. Thomas, W. Zhang, M. E. Kordesch, *Nano Lett* **2006,** *6*, 783.
[11] A. Siems, S. A. L. Weber, J. Boneberg, A. Plech, *New Journal of Physics* **2011,** *13*, 043018.
[12] J. Shah, S. Park, S. Aglyamov, T. Larson, L. Ma, K. Sokolov, K. Johnston, T. Milner, S. Y. Emelianov, *J Biomed Opt* **2008,** *13*, 034024.
[13] G. Baffou, M. P. Kreuzer, F. Kulzer, R. Quidant, *Opt. Express* **2009,** *17*, 3291.
[14] a) A. Gupta, R. S. Kane, D.-A. Borca-Tasciuc, *Journal of Applied Physics* **2010,** *108*, 064901; b) L. M. Maestro, P. Haro-Gonzalez, J. G. Coello, D. Jaque, *Appl. Phys. Lett.* **2012,** *100*, 201110; c) M. L. Debasu, D. Ananias, I. Pastoriza-Santos, L. M. Liz-Marzan, J. Rocha, L. D. Carlos, *Advanced Materials* **2013,** *In press*.
[15] C. D. Jones, L. A. Lyon, *Macromolecules* **2000,** *33*, 8301.
[16] M. Das, N. Sanson, D. Fava, E. Kumacheva, *Langmuir* **2007,** *23*, 196.
[17] a) M. Karg, I. Pastoriza-Santos, J. Perez-Juste, T. Hellweg, L. M. Liz-Marzan, *Small* **2007,** *3*, 1222; b) S. R. Sershen, S. L. Westcott, N. J. Halas, J. L. West, *Journal of Biomedical Materials Research* **2000,** *51*, 293.
[18] a) K. Svoboda, S. M. Block, *Opt Lett* **1994,** *19*, 930; b) J. R. Arias-Gonzalez, M. Nieto-Vesperinas, *J Opt Soc Am A Opt Image Sci Vis* **2003,** *20*, 1201.
[19] a) P. M. Hansen, V. K. Bhatia, N. Harrit, L. Oddershede, *Nano Lett* **2005,** *5*, 1937; b) L. Bosanac, T. Aabo, P. M. Bendix, L. B. Oddershede, *Nano Lett* **2008,** *8*, 1486; c) S. Hormeno, N. G. Bastus, A. Pietsch, H. Weller, J. R. Arias-Gonzalez, B. H. Juarez, *Nano Lett* **2011,** *11*, 4742.
[20] J. Rodriguez-Fernandez, M. Fedoruk, C. Hrelescu, A. A. Lutich, J. Feldmann, *Nanotechnology* **2011,** *22*, 245708.
[21] a) A. Kyrsting, P. M. Bendix, D. G. Stamou, L. B. Oddershede, *Nano Letters* **2010,** *11*, 888; b) H. Mao, J. R. Arias-Gonzalez, S. B. Smith, I. Tinoco, Jr., C. Bustamante, *Biophys J* **2005,** *89*, 1308.
[22] S. Hormeno, B. Ibarra, F. J. Chichon, K. Habermann, B. M. Lange, J. M. Valpuesta, J. L. Carrascosa, J. R. Arias-Gonzalez, *Biophys J* **2009,** *97*, 1022.
[23] M. Honda, Y. Saito, N. I. Smith, K. Fujita, S. Kawata, *Optics Express* **2011,** *19*, 12375.
[24] B. E. A. Saleh, M. C. Teich, *Fundamentals of Photonics*. 3 ed.; John Wiley & Sons: New York, **2007**.
[25] a) L. Ionov, M. Stamm, S. Diez, *Nano Lett* **2006,** *6*, 1982; b) R. Pelton, *Advances in Colloid and Interface Science* **2000,** *85*, 1; c) B. W. Garner, C. Tong, S. Ghosh, Z. Hu, A. Neogi, *Applied Physics Express* **2009,** *2*, 057001; d) S. Schmidt, H. Motschmann, T. Hellweg, R. von Klitzing, *Polymer* **2008,** *49*, 749; e) A. Sanchez-Iglesias, M. Grzelczak, B. Rodriguez-Gonzalez, P. Guardia-Giros, I. Pastoriza-Santos, J. Perez-Juste, M. Prato, L. M. Liz-Marzan, *ACS Nano* **2009,** *3*, 3184.
[26] H. C. van de Hulst, *Light Scattering by Small Particles*. 3 ed.; Dover: New York, **1981**.
[27] P. B. Johnson, R. W. Christy, *Phys. Rev. B* **1972,** *6*, 4370.
[28] A. L. Aden, M. Kerker, *Journal of Applied Physics* **1951,** *22*, 1242.
[29] a) M. C. Wang, G. E. Uhlenbeck, *Reviews of Modern Physics* **1945,** *17*, 323; b) K. Berg-Sorensen, H. Flyvbjerg, *Reviews of Scientific Instruments* **2004,** *75*, 594.

[30] W. Andra, C. G. d'Ambly, R. Hergt, I. Hilger, W. A. Kaiser, *Journal of Magnetism and Magnetic Materials* **1999,** *194*, 197.
[31] J. V. Sengers, J. T. R. Watson, *Journal of Physical and Chemical Reference Data* **1986,** *15*, 1291.
[32] a) O. Andersson, G. P. Johari, *J Chem Phys* **2011,** *134*, 124903; b) F. Arai, C. Ng, H. Maruyama, A. Ichikawa, H. El-Shimy, T. Fukuda, *Lab Chip* **2005,** *5*, 1399; c) J. M. P. Coelho, M. A. Abreu, F. Carvalho Rodrigues, *Optics and Lasers in Engineering* **2004,** *42*, 27; d) S. R. Davidson, M. D. Sherar, *Int J Hyperthermia* **2003,** *19*, 551.
[33] a) T. Hoare, R. Pelton, *Current Opinion in Colloid & Interface Science* **2008,** *13*, 413; b) S. Carregal-Romero, N. J. Buurma, J. Perez-Juste, L. M. Liz-Marzán, P. Hervés, *Chemistry of Materials* **2010,** *22*, 3051.
[34] K. P. Murphy, E. Freire, *Adv. Protein Chem.* **1992,** *43*, 313.
[35] a) J. Evans, Y. Sun, B. Senyuk, P. Keller, V. Pergamenshchik, T. Lee, I. Smalyukh, *Phys Rev Lett* **2013,** *110*, 187802; b) Y. Sun, J. Evans, T. Lee, B. Senyuk, P. Keller, S. He, I. Smalyukh, *Appl Phys Lett* **2012,** *100*, 241901.
[36] R. Contreras-Cáceres, J. Pacifico, I. Pastoriza-Santos, J. Pérez-Juste, A. Fernández-Barbero, L. M. Liz-Marzán, *Advanced Functional Materials* **2009,** *19*, 3070.
[37] S. B. Smith, Y. Cui, C. Bustamante, *Methods Enzymol* **2003,** *361*, 134.